Fourier Transform Spectroscopy of Magnetic Materials

at Terahertz Frequencies

M R F Jensen[1], S A Feiven[2], T Dumelow[3], T J Parker[4]*,
Kamsul Abraha[5], R E Camley[6], S R P Smith[4] and D R Tilley[4]

Department of Physics, University of Essex, Colchester CO4 3SQ, UK

*E-mail: etpkr@yahoo.co.uk

Abstract: We describe a novel high resolution Fourier transform spectrometer and present a brief review of calculated and measured spectral features due to bulk and surface magnetic excitations in insulating and conducting magnetic materials at terahertz frequencies.

1. Introduction

In a recent article in this journal [1] a brief review was presented of the techniques of dispersive Fourier transform spectroscopy (DFTS), polarised oblique incidence reflection spectroscopy and attenuated total reflection (ATR) spectroscopy, and applications of these techniques to a variety of solids were discussed, including alkali halide crystals, pseudo-displacive ferroelectrics, and bulk and low-dimensional semiconductors.

In this article we discuss applications of power Fourier transform spectroscopy and ATR to insulating and conducting magnetic media. If we consider surface modes in magnetic media from an experimental point of view, we discover that the materials pose two well defined measurement problems. The magnetic modes, and hence the associated reststrahl reflection bands, in insulating materials like MnF_2 and FeF_2 have very narrow line widths, ~0.3 cm^{-1}. Surface magnetic polariton modes lie within these narrow reststrahl bands, so that observation of these surface modes requires measurements at high resolution (~10^{-2} cm^{-1}). In conducting magnetic media, on the other hand, e.g. Cr, and the rare earth metals such as Dy and Ho, the conductivity is very high, leading to a reflectivity greater than 99.5%. In such materials the high reflectivity due to the free carriers screens coupling of the incident beam to the magnetic modes and specialised techniques are required to achieve coupling.

If the far infrared dielectric responses of dielectric and magnetic materials are compared, it is found that the associated far infrared reflectivity has an interesting and little-known symmetry property. In the general case of a magnetic medium, i.e. a medium in which the complex permeability, $\mu(\omega) \neq 1$, and the complex permittivity, $\varepsilon(\omega) \neq 1$, the Fresnel reflectivity at normal incidence has the form

$$R(\omega) = \left[\frac{\sqrt{\mu(\omega)} - \sqrt{\varepsilon(\omega)}}{\sqrt{\mu(\omega)} + \sqrt{\varepsilon(\omega)}} \right]^2 \qquad (1)$$

In the case of a non-magnetic lattice, i.e. a simple dielectric with $\mu(\omega) = 1$, the reflectivity has the form

$$R(\omega) \;=\; \left[\frac{1 \;-\; \sqrt{\varepsilon(\omega)}}{1 \;+\; \sqrt{\varepsilon(\omega)}}\right]^2 \tag{2}$$

In the case of a magnetic material the magnetic resonance frequencies are usually found well below the lattice resonance frequencies. To a good approximation $\varepsilon \sim$ constant in the narrow region of the magnetic resonance and for the purposes of illustration can be set to unity, so that

$$R(\omega) \;=\; \left[\frac{\sqrt{\mu(\omega)} \;-\; 1}{\sqrt{\mu(\omega)} \;+\; 1}\right]^2 \tag{3}$$

It can be seen from Eqs. 2 and 3 that the symmetry of the reflectivity as a function of frequency for the magnetic and dielectric response functions is reversed. This feature is often a helpful guide in the identification of magnetic modes and is illustrated in Fig. 1 using data
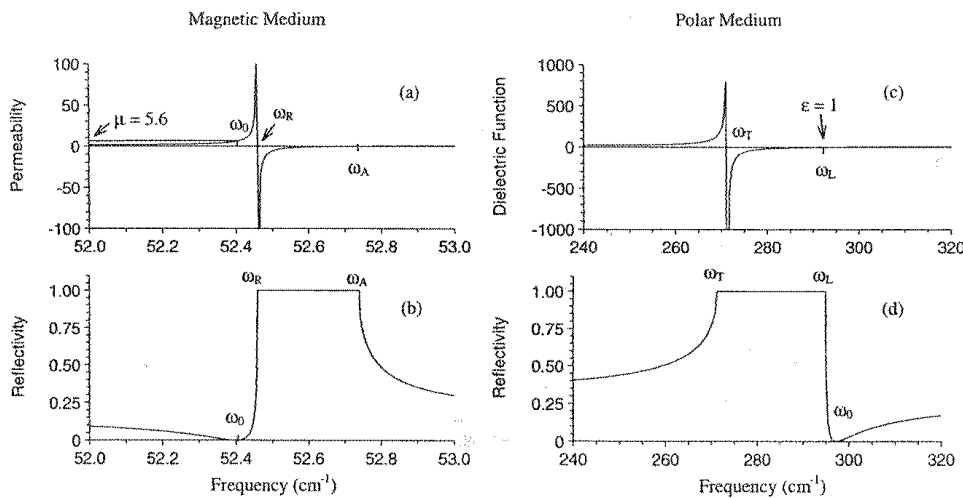

Fig. 1 Illustration of the contrasting symmetries of the reflectivity for a magnetic medium (left) and a dielectric (polar) medium (right). (a) The magnetic permeability of FeF_2, (b) the reflectivity near the magnetic resonance frequency, (c) the dielectric function of GaAs and (d) the reflectivity in the restrahl region. The parameters used in (a) and (b) are for FeF_2: $\omega_R = 52.46\ cm^{-1}$, $\omega_A = 52.74\ cm^{-1}$ and $\varepsilon = 5.6$. The parameters for (c) and (d) are for GaAs: $\omega_T = 271.3\ cm^{-1}$, $\omega_L = 296.0\ cm^{-1}$ and $\varepsilon_\infty = 10.9$.

for FeF_2 and GaAs. Also apparent from Fig. 1 is the very narrow line width, $\sim 0.3\ cm^{-1}$, of magnetic resonance features in insulating magnetic media like FeF_2, which contrasts strongly with the large bandwidth, $\sim 30\ cm^{-1}$, in binary semiconductors like GaAs. Surface magnetic polariton modes can only occur within the narrow bandwidth of the reststrahl band where $\mu < 0$, so, to observe them, a high resolution instrument is required.

Another interesting difference between magnetic and dielectric materials which will be discussed later is that in magnetic materials the reflectivity can demonstrate strikingly non-

reciprocal behaviour under an applied magnetic field, which means that the reflectivity can change dramatically if the applied field is reversed.

In this article we review briefly calculated and measured data for FeF_2, followed by a selection of calculated data on conducting magnetic materials, and measured ATR spectra for the rare earth metal Dy.

2. Instrumentation

A high resolution Fourier transform spectrometer [2] with a liquid helium-cooled ATR stage capable of operating at temperatures down to 1.6 *K* was constructed for measurements on surface magnetic polaritons in insulating magnetic materials like FeF_2, as shown schematically in Fig. 2. It can be seen from the drawing that the layout of the instrument appears to be fairly conventional, but it contains many novel design features, as follows.

(i) The "fixed" mirror is vibrated to provide phase modulation for the infrared beam, and the infrared interferogram is recorded using a liquid helium-cooled bolometer. Phase modulation gives a significant improvement in signal to noise ratio compared with other modulation techniques [2].

(ii) The moving mirror is mounted on a high precision hydraulic drive which provides a maximum mirror travel of 1 *m* to achieve a maximum resolution of 10^{-2} cm^{-1}.

(iii) A helium-neon laser beam is passed along the optic axis of the interferometer. The laser beam is reflected away from the fixed mirror of the interferometer and reflected back along the optic axis by a small side mirror. This arrangement enables different modulation techniques to be used for the far infrared and laser beams.

(iv) The moving mirror is scanned continuously to modulate the output from the laser, and the laser fringes are observed using a small photodiode and used to monitor the optical path difference with high precision.

(v) The scan speed of the moving mirror and the vibration frequency of the "fixed" mirror are chosen carefully to provide modulation frequencies for the infrared and laser beams which are well separated. The maximum modulation frequency of the infrared spectral components due to continuous scanning is 6 *Hz* at 100 cm^{-1}, the maximum wave number for the instrument. The phase modulation frequency is 170 *Hz*, and filtering of the bolometer signal is carefully set to avoid any cross talk between the two modulations.

(vi) The beam divider in the interferometer is constructed from a thin sheet of mylar which produces a strongly polarised output beam, the ratio of s:p polarisation (i.e. the ratio of vertical:horizontal polarisation at the beam divider and also at the sample) being approximately 5:1. The wire grid polariser and roof-top mirror between the interferometer and the sample stage can be used to rotate the plane of polarisation so that the strong s-polarised beam from the interferometer can be used to provide both s- and p-polarised beams at the sample. The improvement in the S/N ratio (~ x 5) obtained in this way for p-polarisation measurements (not shown here) easily justifies the slightly more complicated experimental arrangement. Full details are given elsewhere [2].
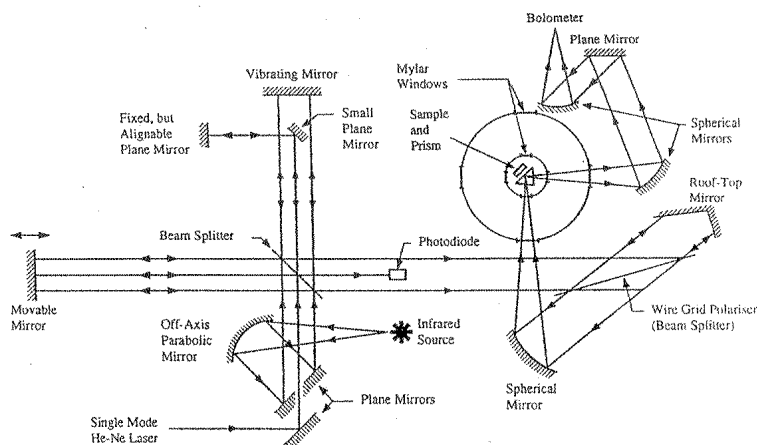
Fig. 2 Schematic diagram of the high resolution Michelson interferometer set up for ATR p-polarised measurements. For further details see [2].

(vii) Measurements can be made either by oblique incidence at 45° angle of incidence, with the sample surface on the axis of the cryostat, or by attenuated total reflection (ATR) spectroscopy with a range of angles of incidence by using prisms cut with different angles.
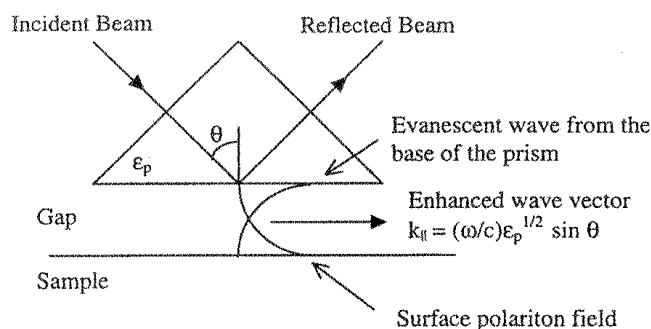

Fig. 3 Schematic diagram of the Otto configuration used for ATR measurements.

   The ATR stage was set up in the Otto configuration [3] on the base of a liquid helium-cooled bolometer as shown schematically in Fig. 3. Radiation is incident on the base of a prism at an angle of incidence greater than the critical angle, θ_c, for total internal reflection given by $\theta_c = \sin^{-1} n^{-1}$, where n is the refractive index of the prism material, in this case Si, for which n = 3.413 and $\theta_c = 17.2^o$ in the far infrared. When the radiation is incident on the base of the prism, an evanescent wave with an enhanced wave vector is set up below the base of the prism. If the sample is placed in an appropriate position near the base of the prism the evanescent wave will couple to both surface and bulk polariton modes in the sample.

3. Magnetic Excitations in insulating media: FeF_2

   We first present calculated magnetic polariton dispersion curves for FeF_2 with and without an applied magnetic field as a guide to the interpretation of the experimental data which are presented later. More details of the calculations are given elsewhere [4-8].

3.1 Calculated magnetic polariton dispersion curves for FeF_2 in zero applied field

Calculated dispersion curves for FeF_2 for the case of zero applied magnetic field are shown in Fig. 4. Bulk modes are confined to the regions bounded by the light curved and horizontal lines and separated by the gap between about 52.5 and 52.8 cm^{-1}. Surface modes lie on the thick lines in the reststrahl region between the two bulk regions, and the very thick curves at the centre of the lower branch of bulk modes describe surface resonant modes. The light lines for reflectivity measurements at 45° angle of incidence are shown as nearly vertical lines, and scan lines for ATR measurements at 30° and 45° angle of incidence are drawn either side of the light lines. It can be seen that the light lines cross the dispersion curves for the resonant modes, but they do not cross the dispersion curves for the surface polaritons. Features from the resonant modes are therefore expected in the reflection spectra, but the surface polariton curves cannot be probed by ordinary reflection measurements. The ATR scan lines on the other hand have sufficiently enhanced wave vectors to intersect the surface polariton curves, so ATR measurements can be used to probe the surface polariton curves.
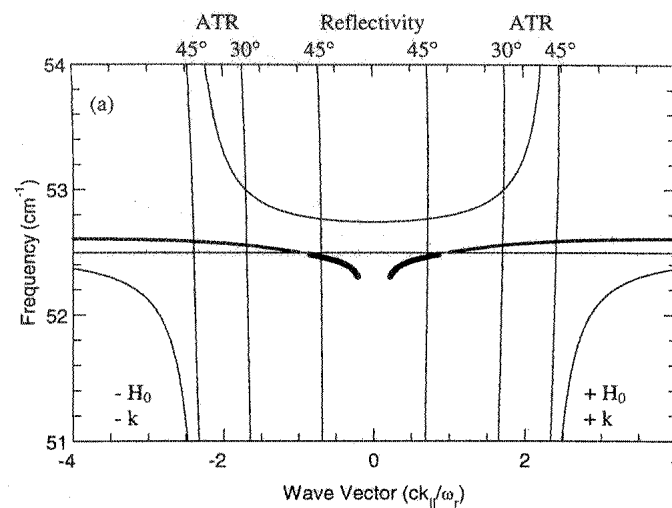

Fig. 4 Calculated s-polarisation dispersion curves for FeF_2 for the case of zero applied field in the Voigt geometry. The bulk regions are bounded by the thin curved and horizontal lines. The surface modes are the thick lines in the reststrahl region between the bulk regions. The scan lines are shown as nearly vertical lines for reflectivity (45°) and ATR (30° and 45°).

3.2 Calculated magnetic polariton dispersion curves for FeF_2 in an applied field

Calculated dispersion curves for FeF_2 in the presence of a small external applied field, $H_o = \pm 0.15$ T, are shown in Fig. 5. It can be seen that due to the Zeeman splitting of the doubly degenerate spin wave there are now three bulk bands, in each case bounded by light curved lines and straight horizontal lines. Furthermore, the symmetry of the surface magnetic polaritons for positive and negative wave vector, $\pm k$, has been destroyed by the applied field. This is striking in each of the reststrahl bands. In the lower reststrahl band the surface polariton branch for $(-H_o, -k)$ is pushed down to very near the top of the bulk band, and the branch for $(+H_o, +k)$ now extends right across the gap. In the upper gap, there is only a surface polariton branch for $(-H_o, -k)$ bounded each end by surface resonant modes. Inspection of the reflectivity light lines and the ATR scan lines and the way they couple to the dispersion curves for both resonant modes and surface polariton modes indicates that different

spectra are now expected for both reflection and ATR measurements for $\pm$ H$_o$. This is therefore the origin of the non-reciprocal behaviour of the reflectivity. Scott and Mills [9] and Camley [10] have explained the non-reciprocal behaviour more fundamentally in terms of the symmetry properties of the system.
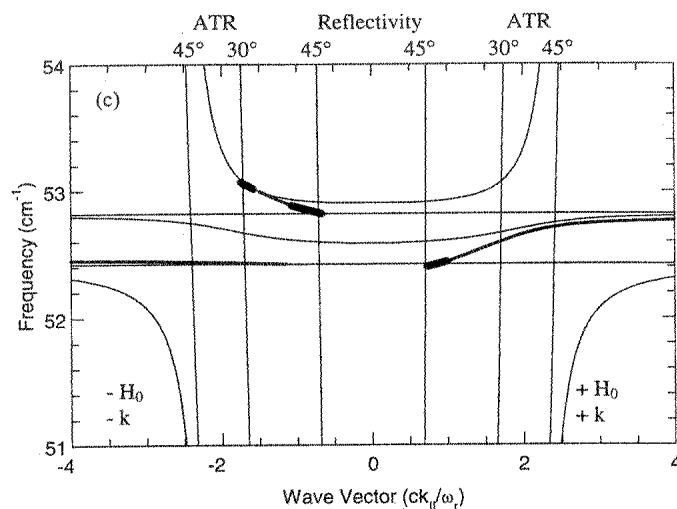

Fig. 5 S-polarisation dispersion curves for FeF$_2$ for H$_o$ = $\pm$ 0.15 T in the Voigt geometry. The bulk regions are bounded by the thin curved and horizontal lines. Surface modes (thick lines) and surface resonances (very thick lines) are also shown. The scan lines are shown as the nearly vertical straight lines, as in Fig. 4.

3.3 Comparison of measured and calculated far infrared spectra of FeF$_2$

(a) Reflection spectrum of FeF$_2$ in zero applied field

Measured and calculated reflectivity spectra for FeF$_2$ in zero applied magnetic field are shown in Fig. 6. First we note that the agreement between measurement and calculation is generally good. Then, comparing these spectra with the calculated spectra for a magnetic medium shown in Fig.1, we see that the line shape has the expected symmetry. The reststrahl band of high reflectivity is well-defined and bounded on the low frequency side by a deep minimum due to coupling to the surface resonance.

(b) Changes to the reflection spectrum of FeF$_2$ in the presence of an applied field

Measured and calculated reflection spectra for FeF$_2$ at 1.7 K in an applied magnetic field of $\pm$ 0.15 T are shown in Fig. 7, and the onset of Zeeman splitting in a low field is clearly visible. There is again good agreement between measured and calculated results, and it is clear that there is now pronounced non-reciprocal behaviour. Comparing these spectra with the positions of the 45° scan lines on the calculated dispersion curves for H$_o$ = $\pm$ 0.15 T shown in Fig. 5 we see two clear reststrahl bands for +H$_o$, together with a surface resonance dip near 52.4 cm^{-1}, consistent with the surface resonance on the 45° reflectivity scan line. For -H$_o$ the lower reststrahl band is more pronounced as there is no surface resonance in the lower gap, but the upper reststrahl band is less pronounced because of the surface resonance at the bottom of the narrow upper gap.
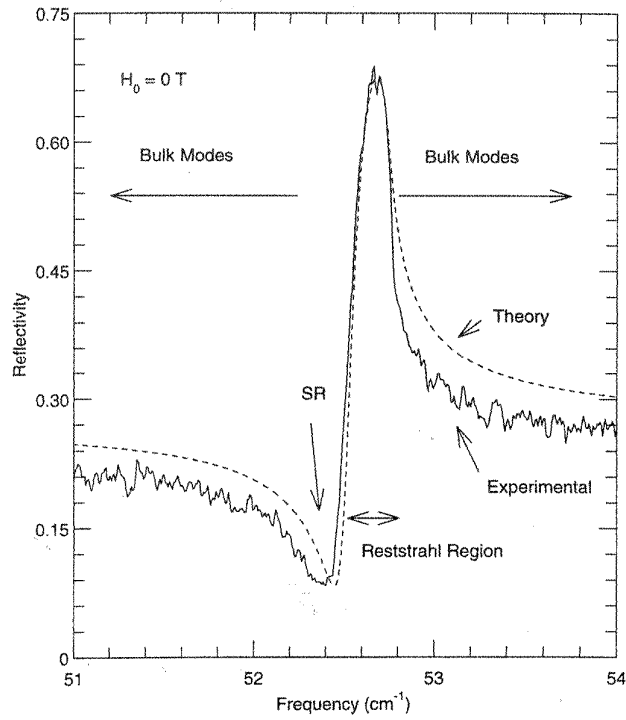
Fig. 6 Measured (solid line) and calculated (dotted line) reflection spectra of FeF_2 with zero applied magnetic field and the easy axis aligned along the z-axis. T = 1.7 K, resolution = 0.02 cm^{-1}.
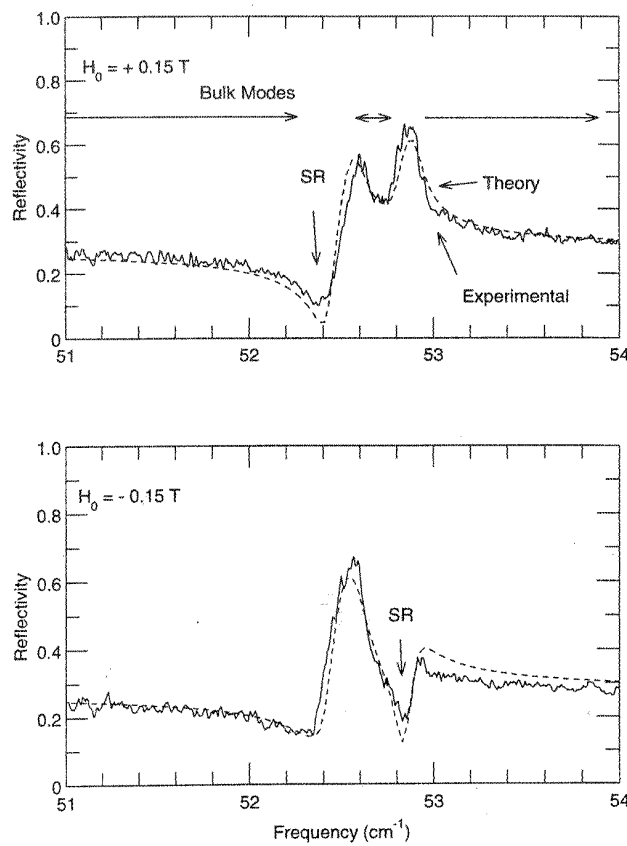

Fig.7 Measured (solid lines) and calculated (dotted lines) reflectivity spectra of FeF_2 at 1.7 K in applied fields of ± 0.15 T. The resolution is 0.02 cm^{-1}. SR marks surface resonances.

(c) ATR spectra of FeF$_2$ in the presence of a magnetic field

Measured and calculated ATR spectra for FeF$_2$ in the Voigt geometry measured in s-polarisation at 1.6 *K* at 30° angle of incidence in applied magnetic fields of ± 0.15 *T* are shown in Fig. 8. The agreement between measured and calculate spectra is again generally very good, and the non-reciprocal behaviour is very clear. The origin of this behaviour can be understood by comparing these spectra with the positions of the two 30° ATR scan lines in Fig. 5. For (+H$_o$, +k), for the 30° ATR scan line the surface polariton is just above the middle of the lower gap, i.e. the lower reststrahl band, leading to a pronounced dip in the ATR spectrum near 52.6 *cm*$^{-1}$. The upper reststrahl band is prominent as it is undisturbed by a surface polariton. For (-H$_o$, -k), the surface polariton mode lies nearly at the lower bound of the lower reststrahl band, leading to a pronounced dip in the ATR reflectivity just above 52.4 *cm*$^{-1}$. The intersection of the 30° scan line with the narrow middle bulk band leads to a weak dip in the ATR reflectivity between 52.7 and 52.8 *cm*$^{-1}$.

4. Magnetic Excitations in Conducting Media

4.1 Phenomenological calculations of the far infrared reflectivity of conducting media

Turning now to conducting magnetic media, we shall see that the high conductivity leads to a quite different measurement problem. In the case of Dy, a rare earth metal, which is ferromagnetic at temperatures below 89 *K*, the ferromagnetic resonance frequency is near 15 *cm*$^{-1}$. The optical constants in the region of the resonance frequency are n ~ 500 and k ~ 700, so that the real part of the far infrared complex permittivity,

$$\varepsilon'(\omega) = n^2 - k^2 \sim -2 \times 10^5 \tag{4}$$

The reflectivity is high at all frequencies below the plasma frequency, which lies in the ultraviolet, and, using the above values of n and k, the background reflectivity in the far infrared,

$$R(\omega) = \left[\frac{N(\omega) - 1}{N(\omega) + 1} \right]^2 \sim 0.997 \tag{5}$$

where the complex refractive index

$$N(\omega) = n(\omega) + ik(\omega) \tag{6}$$

Consequently, the high reflectivity due to the free carriers completely screens coupling of the incident electromagnetic field to the magnetic excitations. For this reason magnetic resonance measurements on conducting media have always presented severe problems.

For measurements on Ni, Dy and Tb, Sievers [11] made far infrared transmission lines by rolling alternate thin layers of metal and polythene sheet into coils. By using a variation of this approach, Camley et al demonstrated theoretically [12] that magnetic resonances are in principle observable by far infrared spectroscopy on suitably structured planar metallic systems where, in a simple reflection experiment on an unstructured sample, the plasma
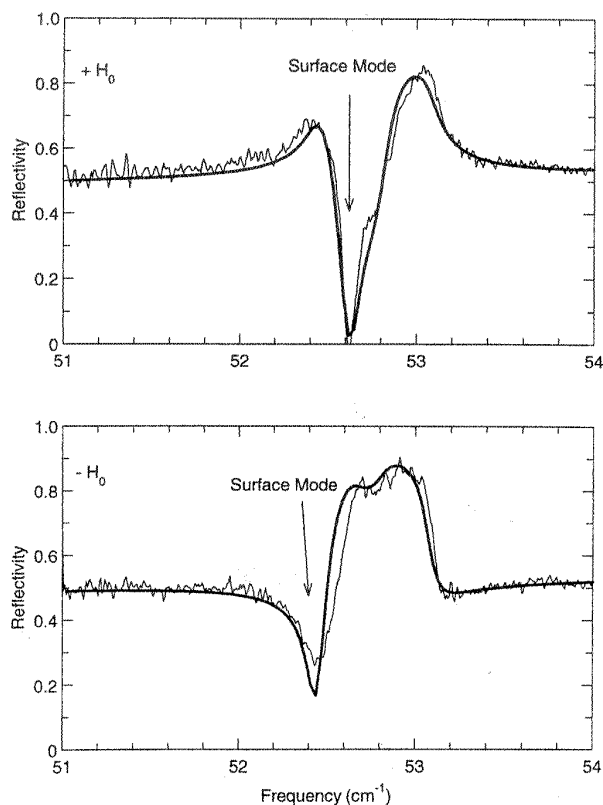
Fig. 8 Measured (thin lines) and calculated (thick lines) ATR spectra for FeF_2 in the Voigt geometry. Temperature = 1.6 K, angle of incidence = 30°, applied field = ± 0.15 T.
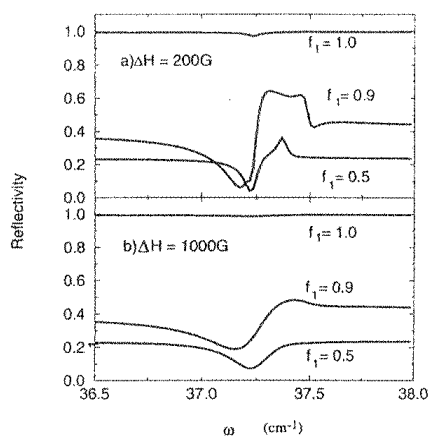

Fig. 9 Calculated reflectivity from an antiferromagnet structured in the form of a grating on a substrate as a function of frequency.

reflectivity would mask the magnetic resonance. They calculated the reflectivity from a sample structured as a grating in which the plasma reflectivity is eliminated by polarising the electromagnetic E-vector normal to the grating and using an angle of incidence of 45°; some of their results are shown in Fig. 9. The results shown in Fig. 9 (a) and (b) correspond to different values of the damping parameter, and the parameter f_1 describes the fraction of the grating period occupied by the sample. In the case of a continuous film ($f_1 = 1.0$), shown for comparison, coupling is barely observable, particularly if there is significant damping, as in (b), and optimum results are obtained with a structured sample when $f_1 \sim 0.9$. It should also

be noticed that the form of the spectra corresponds quite closely to the expected form of the bulk reflectivity due to a magnetic reststrahl band (see Fig. 1) in the absence of any free carrier reflectivity. For the best results such gratings need to be thick (~1-10 μm), with a period of ~ 1 μm, and with very narrow gaps, so they are very difficult to fabricate.

However, Feiven et al [13] have more recently demonstrated by extensive modelling that even greater enhancement of the coupling to the magnetic response is achievable using reflection from a thin grating (thickness ~ 1 μm) placed at the base of a Si prism (in effect, an ATR experiment, though without an air gap). At large angles of incidence, close in effect to the Brewster angle for a Si/metal interface, variations in the permeability $\mu(\omega)$ become significant, and can produce a pronounced magnetic resonance feature with reflectivity changes of the order of 10% at the resonance frequency. Thus a combination of a grating structure to eliminate the plasma reflectivity and careful design to optimise impedance matching produces an enhancement of more than 2 orders of magnitude in the coupling efficiency. This discovery opens the way to the study of most metallic thin film structures. In addition to transition metal structures, such as Cr, we have investigated rare earth metals, as described later.

The advantages which can be achieved are illustrated in Fig. 10, where we compare calculations on five different structures with a nominal resonance frequency of $\omega_m = 38$ cm^{-1}, corresponding closely to Cr. We first consider calculations on continuous Cr films, Fig. 10(a). Curve A shows the reflectivity, R, from a Cr film with a thickness which exceeds the penetration depth (~ 0.3 μm), with the far infrared beam incident at normal incidence (0°) from vacuum; as expected, R ~ 1 throughout. Curve B shows the reflectivity in s-polarisation at 85° angle of incidence, and curve C shows the calculated reflectivity with the far infrared beam incident at an angle of 85° from Si, i.e., an ATR experiment with the Cr sample pressed against the base of a Si prism.
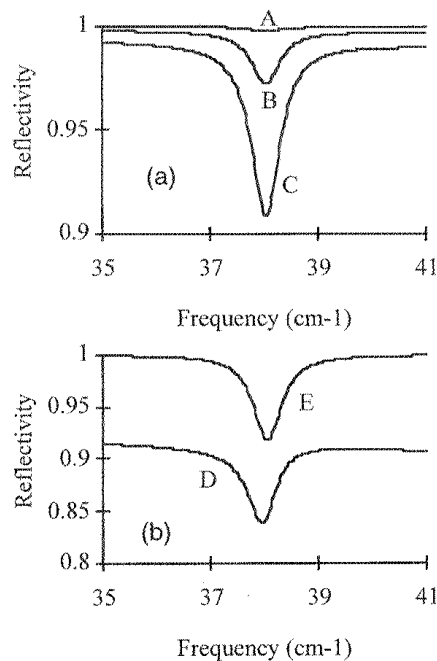

Fig. 10 Calculated reflection spectra of (a) Cr films and (b) Cr gratings. See text for details.

In B and C, the experiments will be relatively difficult to set up because of the large angle of incidence, but the expected enhancements are large. In Fig. 10(b) we show calculations on Cr gratings. Curve D, which has been shifted up by 0.2 for clarity, shows the reflectivity from a grating 10 μm thick deposited on a semi-infinite Si substrate with the far infrared beam incident at 60° from vacuum; an easily measurable signal is calculated, but 10 μm thick Cr films are very difficult to deposit, so the experiment is not compatible with current technology. Finally, in curve E, the reflectivity of a Cr grating of thickness 1 μm on a 2 mm thick quartz substrate with the radiation incident at 60° from a Si prism is shown. The most important advance in curve E is the additional enhancement in coupling efficiency achieved by impedance matching which allows the grating thickness to be reduced to 1 μm. This makes the grating structure practically realisable; we have already used prisms for ATR measurements on FeF_2 with 55° angle of incidence, so all of the experimental conditions corresponding to curve E can be physically realised without difficulty. Moreover, we have been careful to use realistic, rather than optimistic, parameters to model the magnetic resonance; for example, the line width may be less than the assumed value of 0.3 cm^{-1}.

Abraha and Tilley [14] have discussed the far infrared reflectivity of Dy, following earlier work on surface polaritons by Almeida and Tilley [15]. A reflectivity measurement in s-polarisation involves the Voigt permeability and the reflection coefficient for reflection at an interface between media 1 and 2 has the form

$$R = |(1 - f)/(1 + f)|^2 \qquad (7)$$

where f is an appropriate ratio of impedances, i.e. $f = \mu_1 q_2/\mu_2 q_1$, where the normal components of wave vector, q_i, are given by

$$q_i^2 = k_o^2(\epsilon_i \mu_i - \sin^2\theta_o) \qquad (8)$$

where k_o is the wave vector in the external medium and θ_o is the angle of incidence. It can be seen that a low reflectivity will be obtained under the impedance matching condition

$$f \sim 1, \text{ i.e. } \mu_1 q_2 \sim \mu_2 q_1. \qquad (9)$$

If medium 2 is a rare earth metal, the dielectric permittivity ϵ_2 is large and complex, so f is normally large and complex, and R ~ 1. In order that a significant change in reflectivity R is observable, μ_2 needs to be ~ 0. In fact, because of the fact that both ϵ_2 and μ_2 are complex, the maximum change in R occurs when Re$\{\mu_2\}$ is negative, so the observed resonance is technically a surface polariton. Moreover, the larger the value of ϵ_1 (assumed real), the larger the change in R. The above expressions apply to isotropic media; the situation is somewhat more complicated in anistropic media, but for a rare earth metal such as Dy μ_2 can be approximately equated to the Voigt permeability μ_v, and the experimentally observed reflectivity resonance corresponds roughly to a zero in μ_v.

4.2 Far infrared measurements on Dy

Calculations by Abraha and Tilley [14] showed optimum enhancement for rare earth metals with a prism gap of 1 μm, and strong coupling was reported by Feiven et al [16] for Dy with

the sample nominally in contact with (i.e, pressed against) the prism. Measurements were made on a b-cut single crystal of Dy with the sample in the Voigt geometry at 40 *K* using a silicon prism and various values of the applied magnetic field, and a measured ATR spectrum on Dy with an applied magnetic field of 6 *T* is shown in Fig. 11 [16]. The spectrum clearly shows a dip of ~ 25 % in the reflectivity near the resonance frequency with a linewidth of about 2 *cm*$^{-1}$. This is unlike the bulk magnetic reststrahl reflectivity response shown in Figs. 1 and 9 and corresponds to an ATR dip due to coupling to a surface magnetic polariton as explained by Feiven et al [16] (see previous paragraph). Measurements attempted using ordinary oblique-incidence reflectivity showed no observable features at all, corresponding to less than the detectable limit of ~ 0.5%. The improvement in the efficiency of coupling to the resonance using ATR is thus close to two orders of magnitude, although the optimum experimental configuration was very surprising, as discussed below.
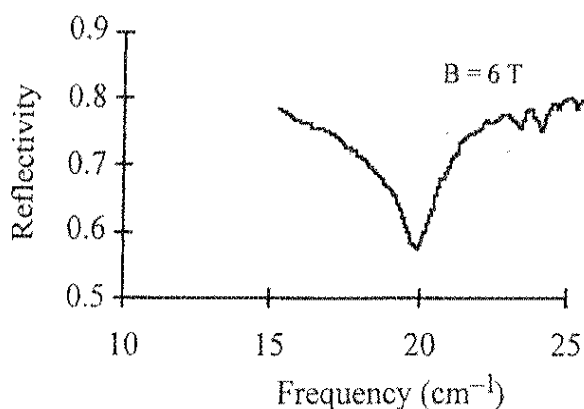

Fig. 11 The measured far infrared ATR spectrum of Dy metal at 40 *K*. Experimental parameters: Si prism, Voigt configuration, 30° angle of incidence, sample in contact with prism, i.e. "nominal" gap close to 1 *μm*. Coupling enhancement ~ x 100 compared with a simple reflection measurement.

A graph of the mode frequency as a function of the applied magnetic field, Fig. 12, shows a field dependence similar to that calculated by Rossol and Jones [17].
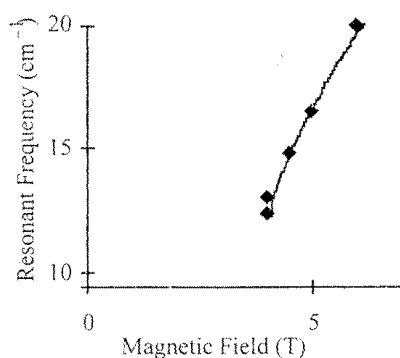

Fig. 12 Dependence of the measured resonance frequency in Dy on the applied magnetic field at T = 40 *K*.

In Table 1 we compare the key parameters for ATR measurements on a polar solid (GaAs), an insulating anitferromagnetic crystal (FeF$_2$) and a highly conducting magnetic material (Dy). Previously, when studying ionic and covalent solids, we have considered that the width of the gap should scale with the wavelength of the surface polariton resonance, as is the case for the

decay length of the evanescent wave at the base of the prism. It can be seen from the table that, although the results for GaAs and FeF_2 roughly follow this trend, the result for Dy certainly does not. We speculate that, for Dy, the mismatch in the optical constants of the prism and the sample (~1:200) is so great that even with a very small gap it is not possible to couple to bulk modes, so there is no possibility of over-coupling even if a very small gap is used to couple to the surface polariton. However, we do not know of any simple systematic arguments relating angles of incidence and ATR gap widths to the physical properties of the various classes of materials. Thus, in this work, in each case the experimental design was based to a large extent on exploratory calculations, and we recommend this approach.

	Polar solid (GaAs)	Insulating AFM (FeF_2)	Rare earth metal (Dy)
Wavenumber, ν	~300 cm^{-1}	55 cm^{-1}	~15 cm^{-1}
Extinction coefficient, k	~8	<1	~500
Wavelength, λ	~30 μm	~180 μm	~650 μm
Gap width, D	~10 μm	~20 μm	~1 μm
D/λ	~1/3	~1/9	~1/650

Tab.1 Comparison of the ATR prism coupling parameters for the cases of a polar solid, and insulating and conducting magnetic media.

5. Conclusions

We have reviewed a selection of calculated and measured far infrared spectra of insulating and conducting magnetic media and demonstrated that magnetic resonance phenomena in both types of material are easily observable. In the case of insulators it is sufficient to use a high resolution instrument, in this case a Fourier transform spectrometer, and prism coupling to observe surface polariton modes. For measurements on magnetic materials with high conductivity more care is required because of the very high reflectivity due to the free carriers. However, we have demonstrated by a combination of calculation and measurement that by using a combination of ATR techniques, samples structured in the form of gratings, and careful design to optimise impedance matching, it is possible to enhance the coupling efficiency by about two orders of magnitude compared with a simple reflectivity measurement. This work demonstrates that screening due to reflection from conduction electrons need no longer be an obstacle to the far infrared or THz spectroscopic investigation of magnetic polariton modes in highly conducting media. This is in striking contrast to the historical perception of spectroscopic investigations of magnetic modes in these materials.

Present addresses of authors:

1: MRFJ: Diamond Light Source Ltd, Oxfordshire, OX11 ODE, UK.

2: SAF: Department of Electronic Engineering, Aston University, Birmingham, B4 7ET, UK.

3: TD: Departamento de Fisica, Universidade do Estado do Rio Grande do Norte (UERN), Costa e Silva, 59610-090 Mossoro RN, Brazil.

4: TJP, SRPS and DRT: Physics Centre, University of Essex, Colchester, CO$ 3JG, UK.

5: KA: Physics Department, Gadjah Mada University, Yogyakarta 55281, Indonesia.

6: REC: Department of Physics, University of Colorado at Colorado Springs, Colorado Springs, CO 80918, USA.

References

[1] T. J. Parker, Fourier transform spectroscopy of solids at terahertz frequencies, *Int. J. THz. Sci. and Techn.*, 2, 75-89, (2009).

[2] D. E. Brown, T. Dumelow, M. R. F. Jensen and T. J. Parker, A high-resolution Fourier transform spectrometer for far infrared magneto-optic spectroscopy of magnetic materials, *Infrared Phys. and Technol.*, 40, 219-230, (1999).

[3] A. Otto, Excitation of non-radiative surface plasma waves in silver by the method of frustrated total reflection, 216, 398-410, *Z. Phys.*, (1968).

[4] M. R. F. Jensen, T. J. Parker, Kamsul Abraha and D. R. Tilley, Experimental observation of surface magnetic polaritons in FeF_2 by attenuated total reflection (ATR), *Phys. Rev. Letts.*, 75, 3756-3759, (1995).

[5] D. E. Brown, T. Dumelow, T. J. Parker, Kamsul Abraha and D. R. Tilley, Non-reciprocal reflection by magnons in FeF_2: A high-resolution study, *Phys. Rev.*, 49, 12266-12269, (1994).

[6] Kamsul Abraha, D. E. Brown, T. Dumelow, T. J. Parker and D. R. Tilley, Oblique-incidence far-infrared reflectivity study of the uniaxial antiferromagnet FeF_2, *Phys. Rev.*, B 50, 6808-6816, (1994).

[7] M. R. F. Jensen, S. A. Feiven, T. J. Parker and R. E. Camley, Experimental determination of magnetic polariton dispersion curves in FeF_2, *Phys. Rev.*, B 55, 2745, (1997).

[8] M. R. F. Jensen, S. A. Feiven, T. J. Parker and R. E. Camley, Experimental observation and interpretation of magnetic polariton modes in FeF_2, *J. Phys. Condens. Matter,* 9, 7233-7247, (1997).

[9] R. Q. Scott and D. L. Mills, Properties of surface magnetostatic waves on ferromagnetic crystal substrates, *Phys. Rev.*, B 5 3545-3557, (1977).

[10] R. E. Camley, Nonreciprocal surface waves*, Surf. Sci. Rep*, 7, 103-187, (1987).

[11] A. J. Sievers, Magnetic resonance in metals in the far infrared, *J. Appl. Phys.*, 41, 980-987, (1970).

[12] R. E. Camley, T. J. Parker and S. R. P. Smith, Reflection of electromagnetic radiation from structured metallic magnets, *Phys. Rev., B* 53, 5481-5487, (1996).

[13] S. A. Feiven, T. J. Parker and S. R. P. Smith, Far infrared investigation of magnetic resonance in conducting magnetic thin films, e.g., Cr and the rare earth metals, and insulating films, e.g., NiO, *Proc. 22nd Int. Conf. on Infrared and Mm. Waves*, Wintergreen, Virginia, July 22-25, 1997, Ed. H. P. Freund, pp. 172-173.

[14] Kamsul Abraha and D. R. Tilley, Theory of far infrared reflectivity and surface magnetic polaritons of rare-earth magnets, *Infrared Phys. and Technol.*, 35, 681-699, (1994).

[15] N. S. Almeida and D. R. Tilley, Surface polaritons on antiferromagnetic superlattices, *Sol. State Comm.*, 73,

23-27, (1990).

[16] S. A. Feiven, T. J. Parker, S. R. P. Smith and D. R. Tilley, Investigation of magnetic excitations in rare earth metals by far infrared ATR spectroscopy, *Proc. 23rd Int. Conf. on Infrared and Mm. Waves*, Colchester, Eds. T. J. Parker and S. R. P. Smith, pp. 150-152. September 7-11, (1998).

[17] F. C. Rossol and R. V. Jones, Ultrabroad ferromagnetic resonance in dysprosium metal, *J. Appl. Phys.*, 37, 1227-1229, (1966).